EUMETSAT NWP SAF
NUMERICAL WEATHER PREDICTION

Report of Visiting Scientist mission NWP_VS18_02

Document NWPSAF-MO-VS-057

Version 1.0

21-11-18

Inter-comparison of line-by-line radiative transfer models MonoRTM and AMSUTRAN for microwave frequencies from the Top-Of-Atmosphere

Karen Cady-Pereira[1], Emma Turner[2], and Roger Saunders[2]

1 Atmospheric and Environmental Research (AER), 131 Hartwell Avenue, Lexington, MA 02421, USA

2 Met Office, FitzRoy Road, Exeter EX1 3PB, Devon, UK

Met Office ECMWF Deutscher Wetterdienst Wetter und Klima aus einer Hand DWD METEO FRANCE Toujours un temps d'avance

Inter-comparison of line-by-line radiative transfer models MonoRTM and AMSUTRAN for microwave frequencies from the Top-Of-Atmosphere

Karen Cady-Pereira (AER),
Emma Turner, Roger Saunders (Met Office)

This documentation was developed within the context of the EUMETSAT Satellite Application Facility on Numerical Weather Prediction (NWP SAF), under the Cooperation Agreement dated 7 December 2016, between EUMETSAT and the Met Office, UK, by one or more partners within the NWP SAF. The partners in the NWP SAF are the Met Office, ECMWF, DWD and Météo France.

Change record			
Version	Date	Author / changed by	Remarks
0.1	02/11/18	K. Cady-Pereira	Draft version
0.2	16/11/18	K. Cady-Pereira	Incorporated comments from E. Turner and R. Saunders
1.0	21/11/18	K. Cady-Pereira	Final version

Inter-comparison of line-by-line radiative transfer models MonoRTM and AMSUTRAN for microwave frequencies from the Top-Of-Atmosphere

1. Introduction

This report describes the results of collaboration between Ms. Karen Cady-Pereira and Dr. Emma Turner at the Met Office during September 3-7, 2018. The objective was to compare MonoRTM, which is developed at Atmospheric Environmental Research (AER) in Cambridge, USA, with the Met Office's AMSUTRAN radiative transfer codes, originally in their native forms, and additionally with a version of AMSUTRAN modified to replicate components of the MonoRTM code. The comparison would allow quantification of the absolute differences between the original codes, verify the components of the modified version of AMSUTRAN and determine if these changes improved agreement between the output from these programs, which finally would allow the cause of any residual differences to be speculated upon.

2. Motivation

Intercomparison of radiative transfer models is a highly useful exercise for quantification of uncertainties in the model physics, development and recommending improvements, and for a general sanity check of absolute results (Melsheimer et al. 2005). AMSUTRAN was developed for the purposes of generating satellite channel-averaged transmittances for the operational fast model RTTOV. It is based on the MPM89 model (Liebe 1989) and has undergone relatively few modifications in the 20 years of its operation. The forthcoming ICI satellite instrument (Thomas 2014) will contain channels extending to 664 GHz, which raises the requirements for accurate simulation beyond 200 GHz, the spectral domain of the current fleet of atmospheric satellite instruments. Investigations are underway at the Met Office to improve the sub-millimeter spectroscopy, where water vapor lines and continuum are the dominant component. The extensive line-by-line models developed at AER follow a rigorous verification procedure by applying empirical constraints from atmospheric observational campaigns. The far-IR spectra region makes a significant contribution (40% of OLR) to the total thermal energy emitted by the Earth (Figure 1, top panel), but until recently there were unacceptably large uncertainties in the spectroscopic parameters of this region, and the adjacent submillimeter region, which is important for water vapor retrievals. This situation was due to the lack of sensitivity in typical atmospheric conditions to the spectroscopic parameters in these spectral ranges (Figure 1, bottom panel); extremely dry conditions were required to provide the necessary data. To this purpose the Atmospheric Radiation Measurement (ARM) programs organized two Radiative Heating in Underexplored Bands Campaigns (RHUBC) campaigns: on the North Slope of Alaska in 2007 and on Cerro Toco in the Atacama Desert in Chile in 2009 (see Delamere et al. 2010, Mlawer et al., 2012, Mlawer et al. 2018). These campaigns deployed multiple radiometers in the microwave, submillimeter, far-IR and mid-IR, and both provided the measurements needed to improve the spectroscopy, and to validate it through radiative closure experiments. This work led to improved water vapor and oxygen line parameters and to an updated continuum model, MT_CKD_3.2, which were included in the MonoRTM version (5.4), the version deployed at the Met Office in September 2018.

3. Approach

Four profiles were selected to span the range in temperature and water vapor of the Earth's atmosphere (Figure 2). The most tropical profile (GARAND_30) had a surface temperature over 300 K and 6.6 cm PWV, while equivalent values for the most arctic profile (GARAND_31) were 250 K and 0.17 cm PWV. MonoRTM was used to calculate the layer amounts for each profile, which were then input into AMSUTRAN, bypassing the AMUSTRAN layer calculation . The impact of the different layering calculations is discussed in the results section.

The original configuration of AMSUTRAN (base) included the following spectroscopy:

- Liebe 89' water vapor lines (30) (Liebe, 1989)
- Tetryakov 05' oxygen lines (44) (Tetryakov et al. , 2005)
- HITRAN 2000 ozone lines (30) (Rothman et al., 2003)
- Liebe 89' water vapor continuum (Liebe, 1989)
- Liebe 93' nitrogen continuum (Liebe 93')
- Liebe 92' oxygen continuum (Liebe 92')

All AMSUTRAN runs used the Van Vleck-Weisskopf lineshape with a quadratic prefactor. The original configuration does not include a line cutoff. Three components from MonoRTM were incorporated into the modified configuration of AMSUTRAN:

- AER "fast" water vapor lines
- AER "fast" ozone lines
- MT-CKD_3.2 water vapor continuum (Mlawer et al., 2018)

AMSUTRAN's processing of the new line catalogues included a cutoff of 25 cm-1 (750 GHz) from the line center, and subtraction of the plinth, in the same manner as AER, however the lineshape itself was still different as AMSUTRAN does not include Doppler broadening.

Both models use the linear-in-tau approximation to calculate brightness temperature from optical depths/transmittances on layers. All runs were performed for the 0-1000 GHz range, with a resolution of 50 MHz.

4. Results

Brightness temperatures from the AMSUTRAN base runs for the four Garand profiles showed large differences (20K) with respect to MonoRTM for specific lines (e.g., 60 and 120GHz O_2 lines) as well as over extended spectral regions (e.g., between 800 and 900 GHz, where water vapor dominates absorption) (Figure 3). The modified AMSUTRAN runs showed greatly reduced extended biases and some reduced line differences. A blowup of the differences showed that AMSUTRAN still had a systematic negative bias that increased with increasing frequency (Figure 4). This bias was traced back to an error in the partition function. Correcting this error removed the trend and reduced the bias to less than 1.0 K for most of the 0-1000 GHz range (Figure 5).

Total transmittances determine the radiance observed at the instrument, and therefore are a useful parameter for determining the impact of model changes. We analyzed the differences between the base and modified AMSUTRAN surface to space transmittances with respect to MonoRTM (Figure 6). The driest Garand profile (GARAND_31) obviously presented the largest transmittance, and also the largest differences between the base AMSUTRAN run and MonoRTM. The transmittances from the modified AMSUTRAN run showed qualitatively similar decreases in biases as the brightness temperatures from the modified AMSUTRAN run.

A series of MonoRTM and AMSUTRAN base and modified runs were carried out, in which only a subset of molecules or spectroscopic features were turned on in order to isolate dominant components of the total difference. The runs were:

- oxygen and ozone but no water vapor (dry)
- oxygen, lines only
- ozone, lines only
- water vapor, lines only
- water vapor, total continuum only
- water vapor, foreign continuum only
- water vapor, self continuum only

Comparing the total transmittance differences between base and modified AMSUTRAN and MonoRTM. (Figure 7, top two panels) with each of the transmittance components highlights oxygen as a primary contributor: the large spikes being due to missing oxygen lines in AMSUTRAN (Figure 7, fifth and sixth panels). Further analysis based on optical depth differences will be presented below. The inclusion of MonoRTM ozone lines in AMSUTRAN reduced the AMSUTRAN ozone line transmittance differences with respect to MonoRTM from a maximum of -0.8 to -0.2 (Figure 7, seventh and eighth panels).

Adopting MonoRTM water vapor lines reduced the AMSUTRAN water vapor line transmittance differences with respect to MonoRTM from a maximum of 0.15 to ~0.025 (Figure 8, first and second panels). This change had of course the greatest impact on the wettest profile (GARAND_30); but some small but broad differences still remain, most notably between 200 and 300 GHz and 800 and 900 GHz, though the latter is only clearly evident for the driest profile (GARAND_31), which has the highest transmittance. Including the MT_CKD_3.2 continuum basically eliminated transmittance differences due to the water vapor continuum, both in total and decomposed into foreign and self contributors. Interestingly the original Liebe 89' continuum overestimated the foreign and underestimated the self components with respect to MT_CKD_3.2, though differently for the different profiles (Figure 8, third through eighth panels); this difference in behavior is in part due to the increasing importance of the self continuum for wetter profiles, but probably also to the different spectral dependence of the Liebe 89' and MT_CKD_3.2 models. It is also evident that the remaining differences in water vapor transmittances are smooth for modified AMSUTRAN, whereas the remaining ozone differences are very "spiky". We believe this is due to the different spectral interval which in AMSUTRAN is in GHz and in MonoRTM in cm^{-1}. Since the interval is fixed, MonoRTM and AMSUTRAN's spectral grids slightly diverge as frequency increases with an irregular offset with respect to one another, leading to

small offsets. Around the centers of sharp lines this difference is most pronounced (hence the large spikes in the 60 GHz oxygen complex and at 118 GHz). As water vapor is mostly located in the lower troposphere, and ozone in the upper troposphere and lower stratosphere, water vapor lines undergo much greater broadening than ozone lines; therefore the offset is much more visible in the ozone transmittance.

Since large differences in optical depth can appear as small differences in transmittance determining which factors are responsible for these changes can be better accomplished by analyzing optical depths. We examined were the large differences in transmittances at the center of oxygen lines (Figure 9, left panel). We focused on the 61.8 GHz line and found that increasing the spectral resolution of both AMSUTRAN and MonoRTM calculations from 50 MHz to 5 MHz dramatically changed the shape of the optical depth spectrum, as would be expected, but also significantly reduced the peak of the AMSUTRAN line, bringing into much better agreement with the MonoRTM peak value (Figure 9, right panel). The increase in resolution brought the two spectral grids closer to each other at each frequency, so only small differences remain at the peak.

The optical depth differences between AMSUTRAN and MonoRTM (Figures 10 and 11) are at the location of oxygen lines included in MonoRTM but not in AMSUTRAN. The missing lines appear as 100% differences from MonoRTM, and where both models include the line there is some shape distortion, which is possibly due to different line shape calculation algorithms. This is an issue still under investigation. However, as these missing lines have transmittance below 0.15 (see Figure 7, fifth and sixth panels), they will not contribute significantly to the signal at the instrument, but may be responsible for some of the smooth brightness temperature differences in Figure 5 (lower panel) by way of their missing line wings.The spikiness seen in the ozone transmittance differences also appears in the ozone optical depth differences; since these lines are narrow due to ozone's vertical distribution, this is due to the spectral resolution issue discussed above. Additionally the optical depth of ozone is small in itself, so a small change can lead to a relatively large percentage change. The spikiness in the water vapor continuum is an anomalous effect of decomposing MonoRTM optical depths into its component parts and should be ignored as water vapour continuum is a smooth function.

Having avoided the problem of different layer amount calculations by forcing AMSUTRAN to use MonoRTM layer amounts, we returned to this issue and evaluated the impact of the different layering within both the original (Figure 12, top panel) and modified AMSUTRAN (Figure 12, bottom panel) models. The differences can be as large as 1K at line centers, and in modified AMSUTRAN are significant even away from the major lines, as the water and ozone amounts are different

5. Conclusion

The inter-comparison of MonoRTM with AMSUTRAN was successfully implemented and carefully evaluated. After identifying differences associated with a slightly offset spectral grid, modified AMSUTRAN compared extremely well with MonoRTM, except in regions where AMSUTRAN is missing oxygen lines modeled by MonoRTM, and some small residuals which may be associated with lineshape differences. Incorporating these lines is a work-in-progress at the Met Office. Further development of AMSUTRAN to incorporate spectroscopic features of MonoRTM has been shown to be a worthwhile endeavor, and as the latter has been validated in the field on several campaigns, is well placed to help provide more accurate results in retrievals and within forecasting models.

References

Clough, S.A., and M.J. Iacono, Line-by-line calculations of atmospheric fluxes and cooling rates II: Application to carbon dioxide, ozone, methane, nitrous oxide, and the halocarbons. *J. Geophys. Res.*, **100**, 16,519-16,535, 1995.

Delamere, J. S., S.A. Clough, V. H. Payne, E. J. Mlawer, D. D.Turner and R. R. Gamache, A far-infrared radiative closure study in the Arctic: Application to water vapor, *J. Geophys. Res.*, **115**, D17106, doi:10.1029/2009JD012968, 2010.

Liebe H.J., MPM–An atmospheric millimeter-wave propagation model. International Journal of Infrared and millimeter waves, *International Journal of Infrared and Millimeter Waves*, vol.**10,** no.6, pp. 631-650, 1989.

Liebe, H., Rosenkranz, P., and Hufford, G.: Atmospheric 60-GHz oxygen spectrum: New laboratory measurements and line parameters, *Journal of quantitative spectroscopy and radiative transfer*, 48, 629–643, 1992.

Liebe, H., Hufford, G., and Cotton, M.: Propagation modeling of moist air and suspended water/ice particles at frequencies below 1000 GHz, in: *In AGARD, Atmospheric Propagation Effects Through Natural and Man-Made Obscurants for Visible to MM-Wave Radiation* 11 p (SEE N94-30495 08-32), 1993.

Melsheimer, C. et al. Intercomparison of general purpose clear sky atmospheric radiative transfer models for the millimeter//submillimeter spectral range. *Radio Science.,* **vol. 40**, RS1007, doi:10.1029/2004RS003110, 2005

Mlawer et al.: Analysis of water vapor absorption in the far-infrared and submillimeter regions using surface radiometric measurements from extremely dry locations, submitted to *JGR Atmospheres*, 2018.

Mlawer, E.J., V.H. Payne, J.-L. Moncet, J.S. Delamere, M.J. Alvarado, and D.C. Tobin Development and recent evaluation of the MT_CKD model of continuum absorption, *Phil. Trans. R. Soc. A*, **370**, 1–37 doi:10.1098/rsta.2011.0295, 2012.

Rothman et al., The HITRAN molecular spectroscopic database: edition of 2000 including updates through 2001, *J. Quant. Spectrosc. Radiat. Transfer*, **82**,5-44, 2003.

Thomas, B., Brandt, M., Walber, A., Gibson, H., Philipp, M., Sonnabend, G., Benzazaa, M., Gonzalez, R., Bergada, M., Martinez, J., et al. Millimeter & sub-millimeter wave radiometer instruments for the next generation of polar orbiting meteorological satellites-MetOp-SG, in: *Infrared, Millimeter, and Terahertz waves (IRMMW-THz), 2014 39th International Conference on*, pp. 1–3, IEEE, 2014

Tretyakov, M.Y., M.A. Koshelev, V.V. Dorovskikh, D.S. Makarov, and P.W. Rosenkranz: 60-GHz oxygen band: precise broadening and central frequencies of fine-structure lines, absolute absorption profile at atmospheric pressure, and revision of mixing-coefficients, *J. Molec. Spectrosc.*, **231**, 1-14, 2005.

Figures

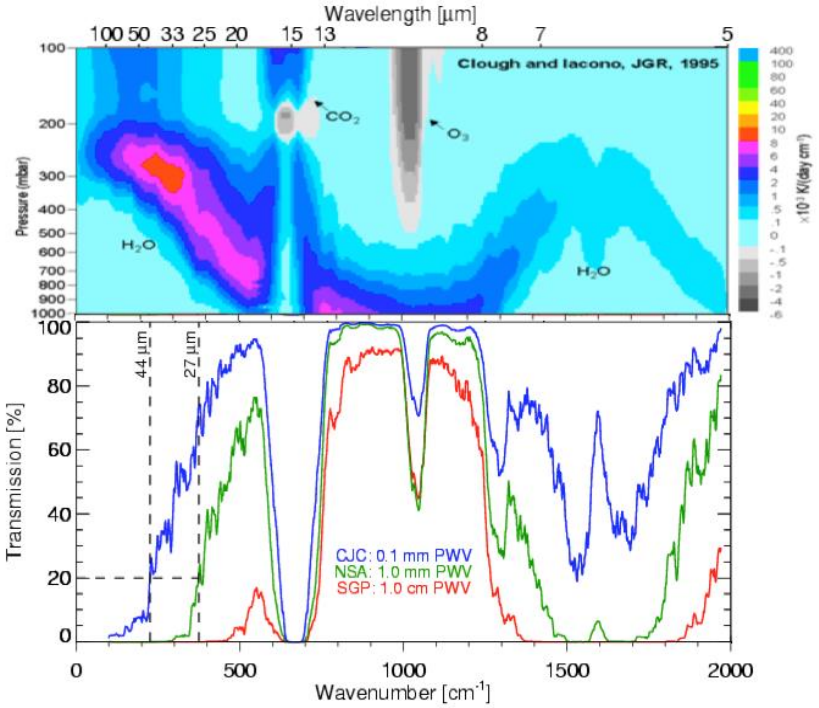

Figure 1: Spectral cooling rates for the mid-latitude summer atmosphere calculated by LBLRTM (top (from Clough and Iacono, 1995)); LBLRTM transmission for profiles from Chajnantor, Chile (CJC) , the North Slope of Alaska (NSA) and the Southern Great Plains (SGP) ARM site

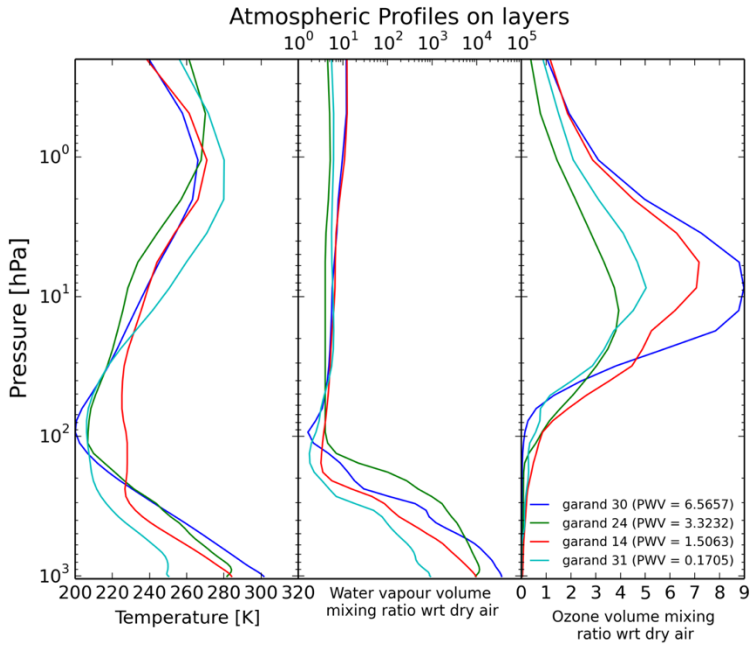

Figure 2: Four Garand profiles selected for AMSUTRAN vs MonoRTM comparisons

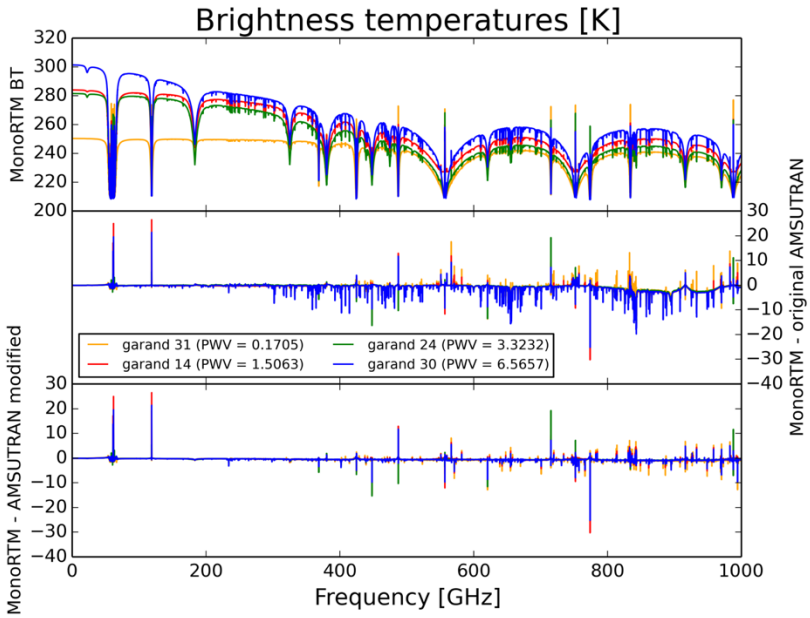

Figure 3: MonoRTM brightness temperature for each of the four test profiles (top); brightness temperature differences: MonoRTM- base AMSUTRAN run (middle); MonoRTM – modified AMSUTRAN (bottom)

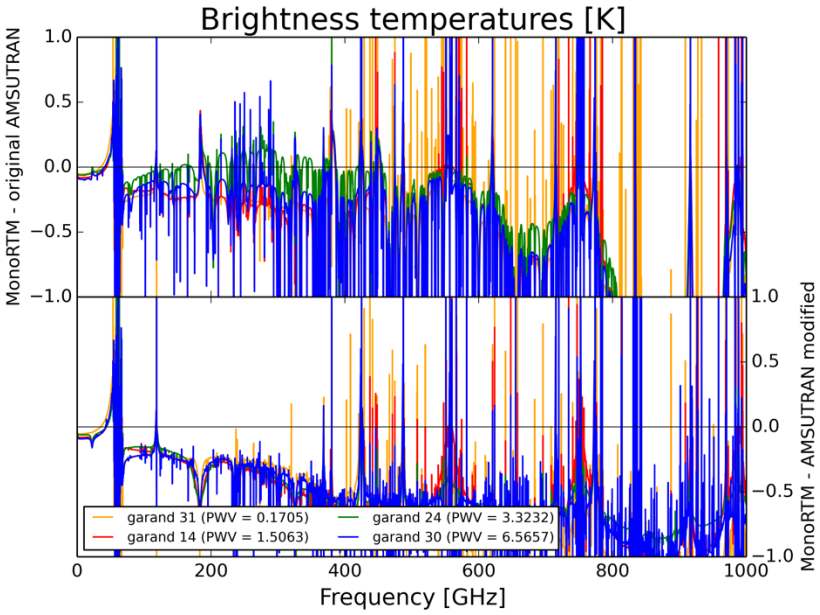

Figure 4: Bottom two panels of Figure3, with smaller y-axis scale

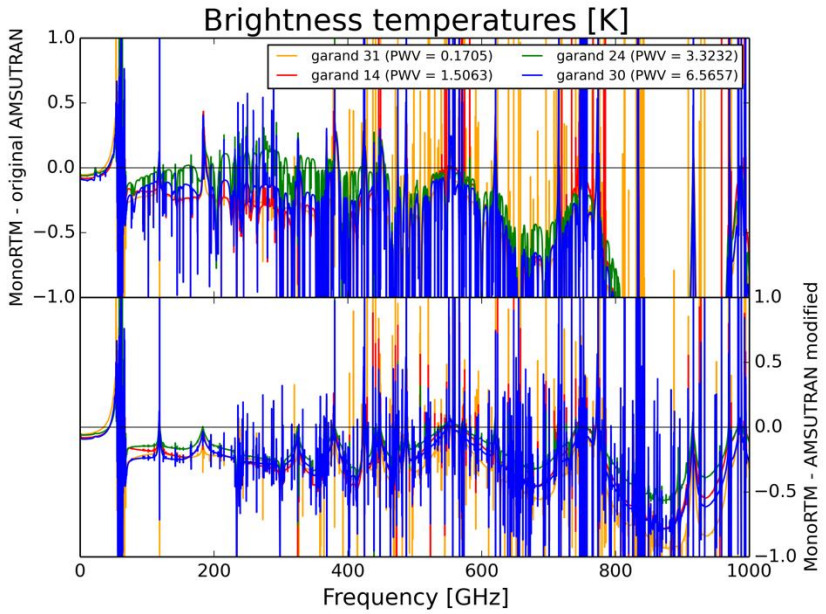

Figure 5: Same as Figure 4, after partition function correction

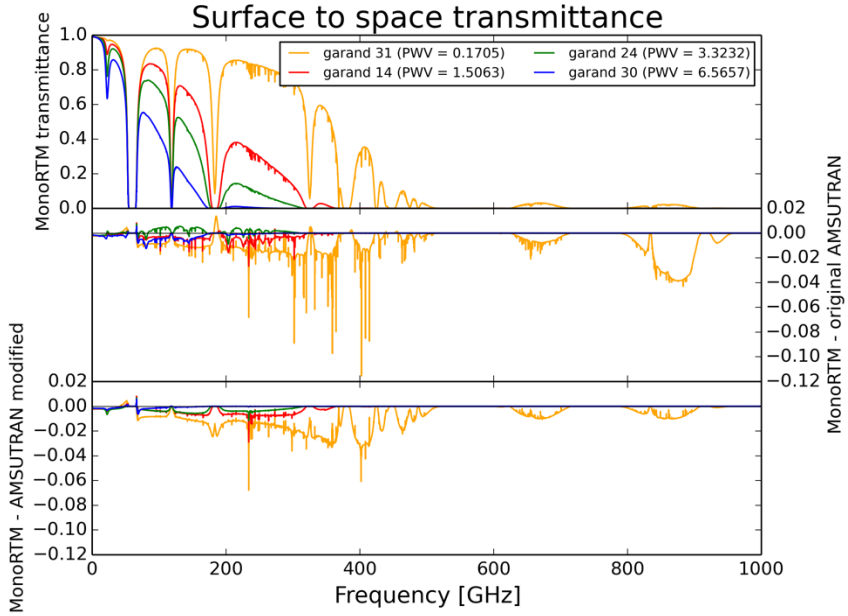

Figure 6: : MonoRTM transmittances for each of the four test profiles (top); transmittance differences: MonoRTM-base AMSUTRAN run (middle); MonoRTM – modified AMSUTRAN (bottom)

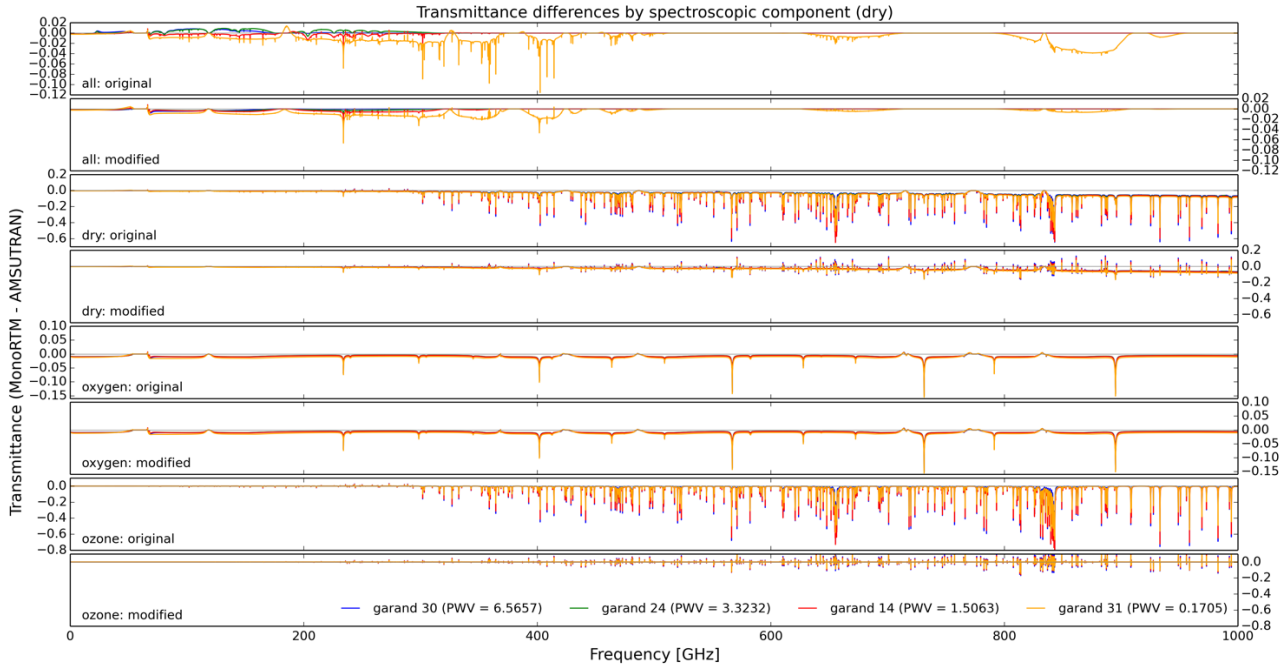

Figure 7:MonoRTM-AMSUTRAN (original and modified) transmittance differences by component: all components (top two panels), all non water vapor components (third and fourth panels, oxygen (fifth and sixth panels), ozone (bottom two panels)

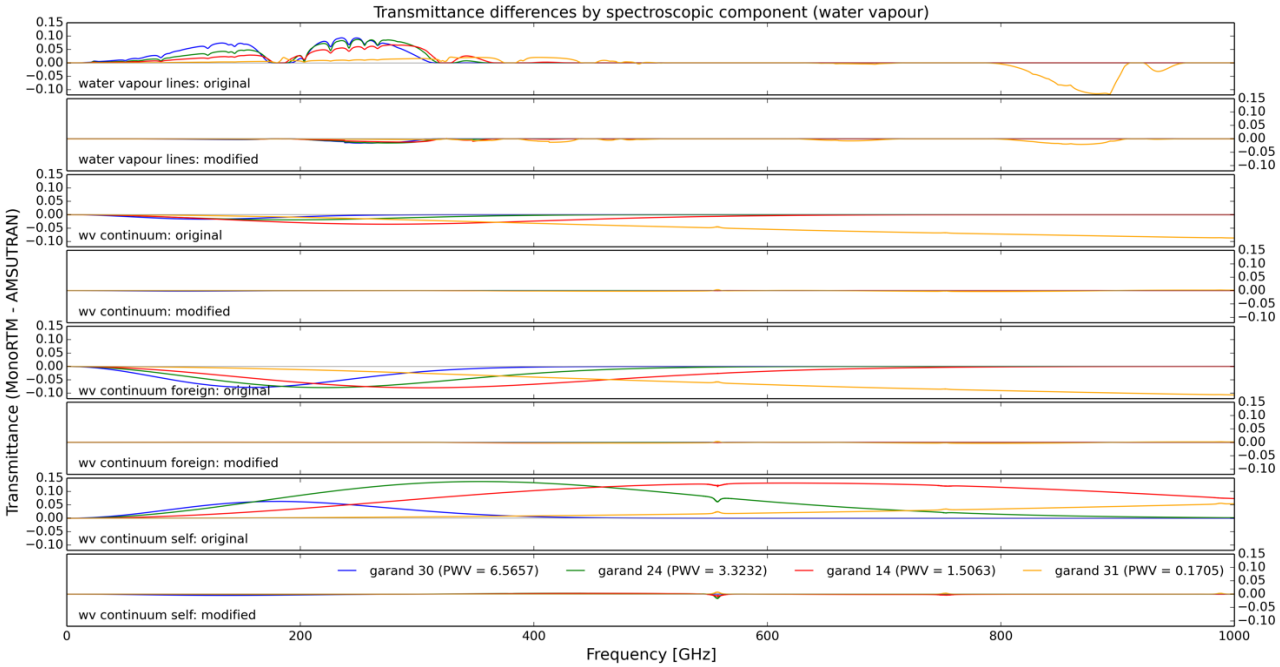

Figure 8: MonoRTM-AMSUTRAN (original and modified) transmittance differences for water vapor: lines (top two panels), total continuum (third and fourth panels), foreign continuum (fifth and sixth panels), self continuum (bottom two panels).

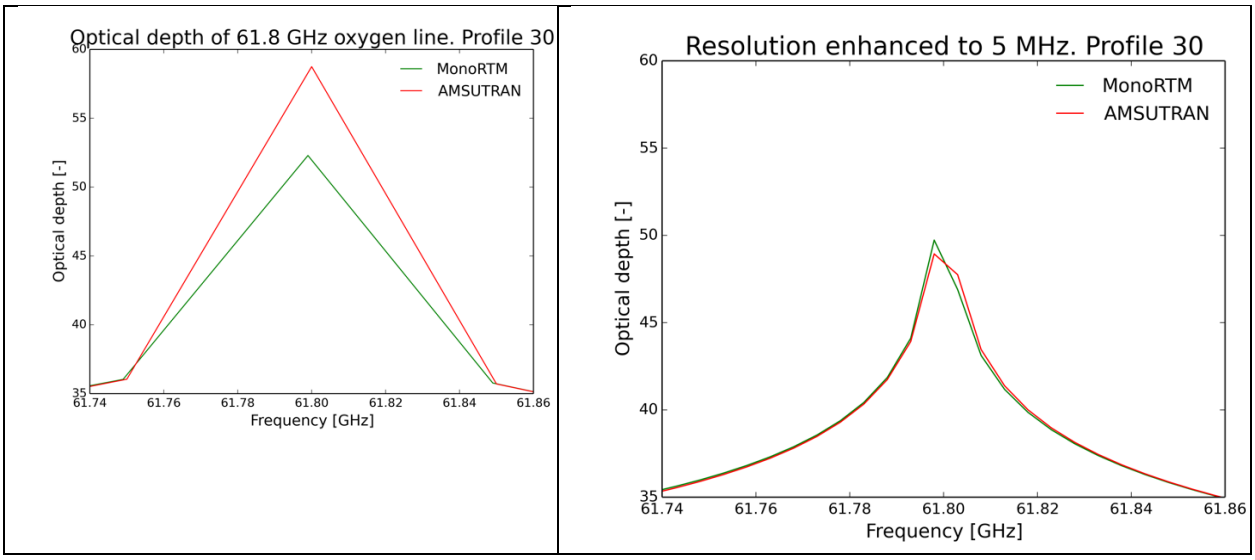

Figure 9: Optical depth of oxygen 61.8 GHz line at 50 MHz resolution (left) and 5 MHz (right).

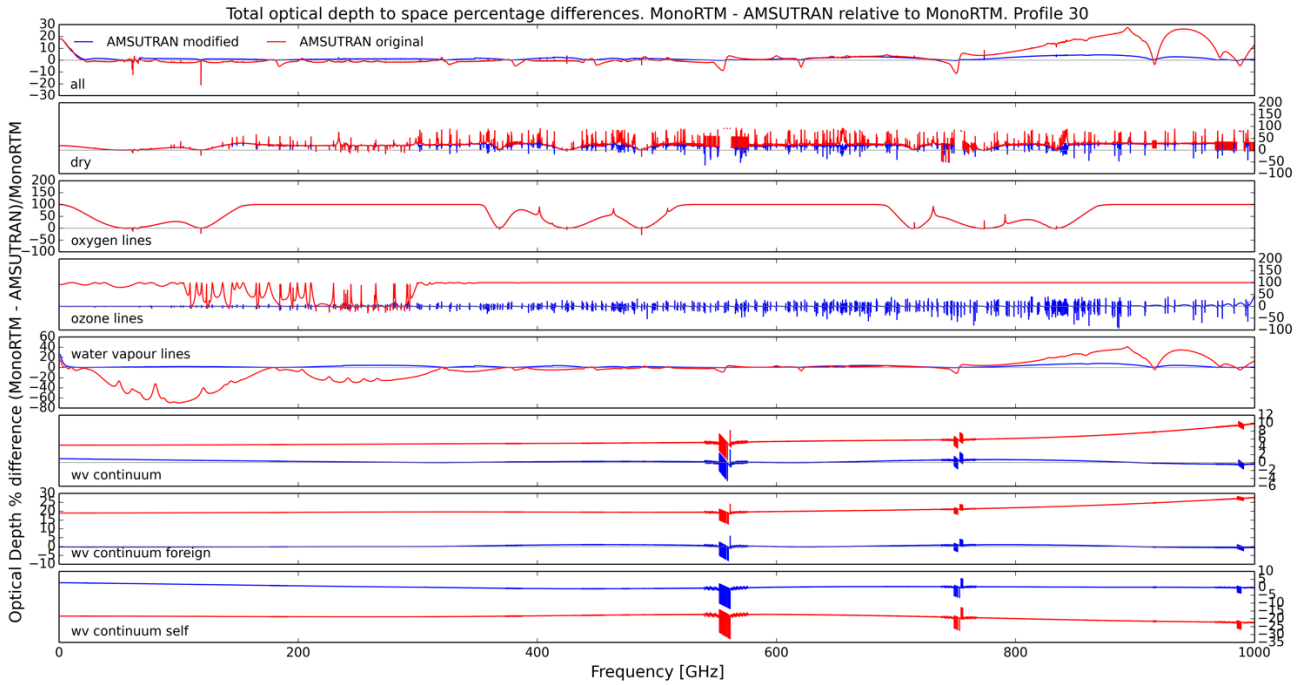

Figure 10: Percentage differences in optical depth between AMSUTRAN (modified and original) and MonoRTM for Garand profile 30

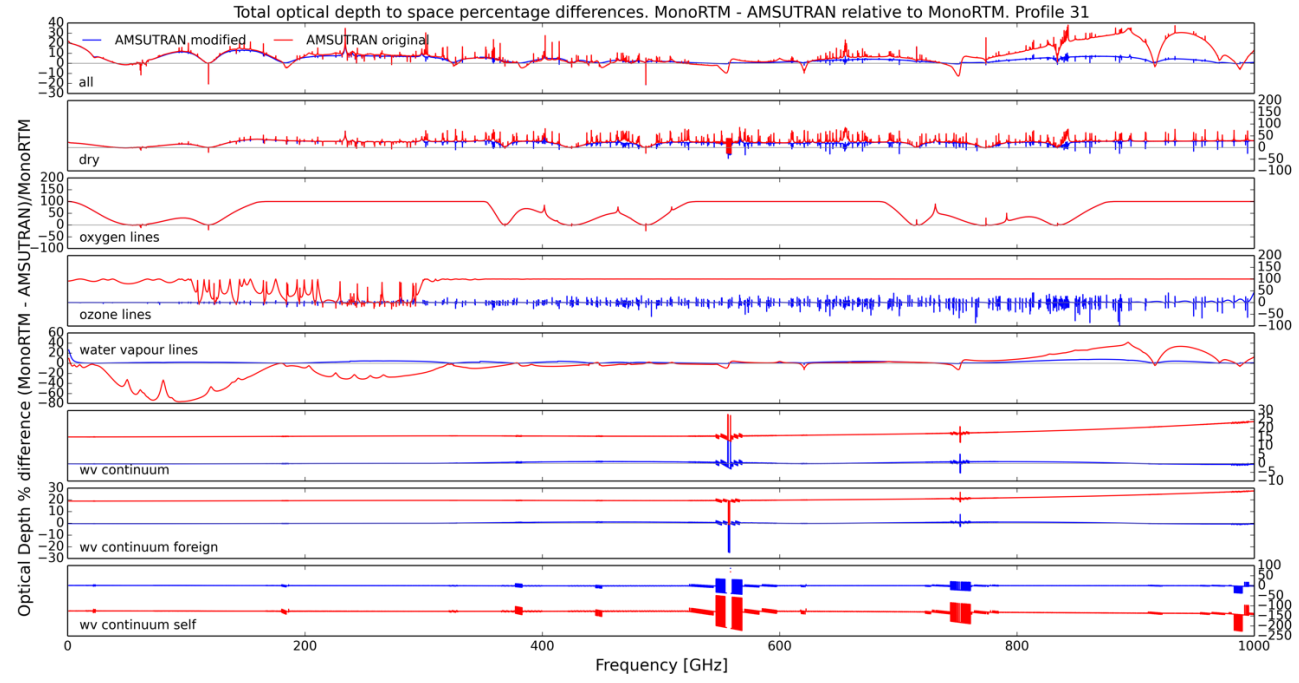

Figure 11: Percentage differences in optical depth between AMSUTRAN (modified and original) and MonoRTM for Garand profile 31

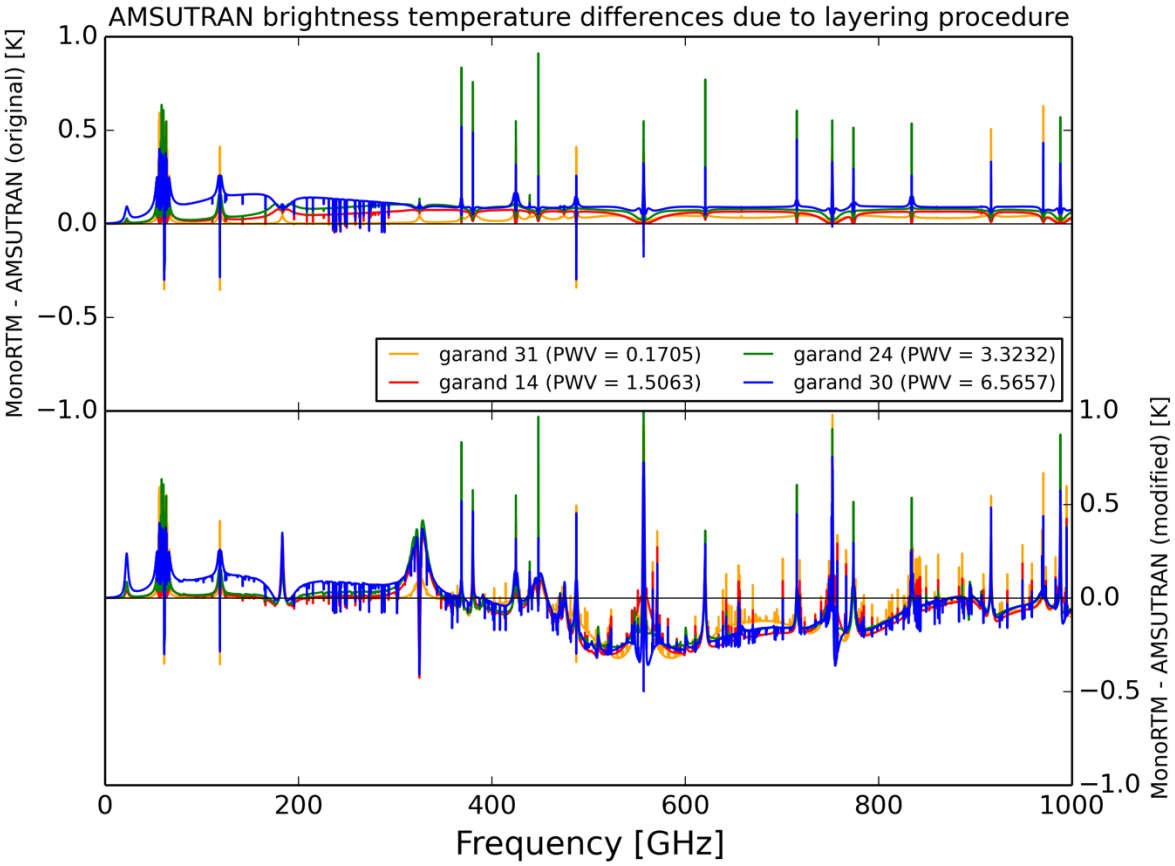

Figure 12: Brightness temperature differences due to different layer amount calculations (MonoRTM-AMSUTRAN): original AMSUTRAN (top), modified AMSUTRAN (bottom).